Journal of Crystal Growth 97 (1989) 235–242
North-Holland, Amsterdam

INFLUENCE OF THE PRANDTL NUMBER ON LAMINAR NATURAL CONVECTION IN A CYLINDER CAUSED BY *g*-JITTER

Stefan SCHNEIDER and Johannes STRAUB

Lehrstuhl A für Thermodynamik, Technische Universität München, Arcisstrasse 21, D-8000 München 2, Fed. Rep. of Germany

A numerical code has been developed to calculate three-dimensional buoyancy-driven convection in a differentially heated cylinder with rigid walls. Using this code the influences of time-dependent residual accelerations in the microgravity environment on board a spacecraft are studied. These accelerations called *g*-jitter might cause convective flow in cavities like the one mentioned above. The ain of this work is to point out the influence of various parameters like the amplitude (expressed by the Rayleigh number Ra*), pulse duration (Fourier number Fo*) or frequency (f), the fluid filling the cylinder (Prandtl number Pr) and the kind of acceleration. The Rayleigh number is varied in the range from 200 to 20000, the Prandtl number in the range of 0.023–135.

1. Introduction

During the last years great efforts were made in materials science on experiments in a microgravity environment. Most of these experimental systems consist of a differentially heated cavity filled with liquid material. Even if the residual accelerations on board a spacecraft on average are fairly small there are many transient accelerations of various amplitudes that might cause non-uniformities in the crystal during a solidification experiment. An experimental study of the influence of such "*g*-jitter" perturbations cannot be carried out under earth conditions and in space it requires much effort. Therefore, numerical calculation of these effects may help to interpret experiments performed in space and to avoid inhomogeneities in the solid or crystal structure when experiments are designed in the future.

Elder [1] and Foster [2] investigated the flow development in an infinite horizontal fluid layer with a vertical temperature gradient due to a sudden change of the bottom wall temperature. Gresho and Sani [3] also studied an infinite horizontal fluid layer with a vertical temperature gradient when the gravitational field consists of a constant part plus a sinusoidally varying part. More recently Monti et al. [4] describe an order of magnitude analysis to estimate the influence of a sudden gravity step under major simplifications. Griffin and Motakef [5] investigated the convection in a vertical cylindrical cavity filled with liquid germanium. Kirchartz [6] and Kirchartz et al. [7] studied the natural convection in a two-dimensional rectangular cavity. They found out that the development time for convection is much shorter in the case of an inclination angle of 90° (horizontal temperature gradient) than for a box with vertical temperature gradient (corresponding to Rayleigh–Bénard or cellular convection). Also the first increase of the flow amplitude is greater by 2 orders of magnitude in the case of the horizontal cavity. Hence, as the *g*-jitter perturbations are typically of short duration, we concentrate on the case of a horizontal cylinder in this study. *g*-Jitter perturbations mostly are of relatively small amplitudes and buoyancy-driven flows are in general three-dimensional in real applications. We have developed a numerical code to calculate three-dimensional laminar natural convection in a cylinder using the experience of many years in developing numerical codes for calculating thermo-fluid-dynamic problems at our institute (e.g., refs. [8,9]). In a former study [10], we

0022-0248/89/$03.50

investigated the influences of single gravity pulses of various amplitudes and durations on air-filled cylinders with different aspect ratios.

2. Theoretical approach

2.1. Physical and mathematical model

The investigated problem is sketched in fig. 1. The time-dependent three-dimensional buoyancy-driven flow in a cylinder (filled with gas or liquid) with constant properties except density is governed by the following equations (compressive work and viscous dissipation neglected):

Equation of continuity:

$$\mathrm{D}\rho/\mathrm{D}t = -\rho(\nabla \cdot \boldsymbol{v}). \tag{1}$$

Equation of motion:

$$\rho \mathrm{D}\boldsymbol{v}/\mathrm{D}t = -\nabla p + \mu\nabla^2\boldsymbol{v} + \rho\boldsymbol{g}. \tag{2}$$

Equation of energy:

$$\rho c_p \, \mathrm{D}T/\mathrm{D}t = k \, \nabla^2 T. \tag{3}$$

Equation of state of an ideal gas:

$$\rho = p/R_0 T. \tag{4a}$$

Linear dependence of density on the temperature (for a liquid):

$$\rho = \frac{\rho_0}{1 + \gamma(T - T_0)}, \tag{4b}$$

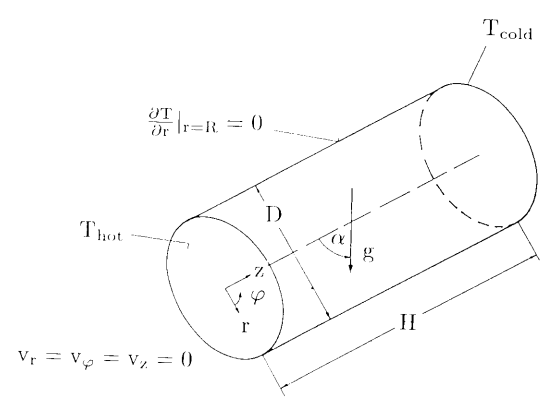

Fig. 1. Schematic diagram of the cylinder and the boundary conditions.

with

$$\frac{\mathrm{D}}{\mathrm{D}t} = \frac{\partial}{\partial t} + v_r\frac{\partial}{\partial r} + \frac{v_\phi}{r}\frac{\partial}{\partial \phi} + v_z\frac{\partial}{\partial z},$$

$$\nabla = \frac{1}{r}\frac{\partial}{\partial r}r + \frac{1}{r}\frac{\partial}{\partial \phi} + \frac{\partial}{\partial z},$$

$$\nabla^2 = \frac{1}{r}\frac{\partial}{\partial r}\left(r\frac{\partial}{\partial r}\right) + \frac{1}{r^2}\frac{\partial^2}{\partial \phi^2} + \frac{\partial^2}{\partial z^2},$$

where ρ denotes the fluid density, $\boldsymbol{v}$ the velocity vector (v_r, v_ϕ, v_z), T the temperature, p the pressure, $\boldsymbol{g}$ the vector of gravitational acceleration (g_r, g_ϕ, g_z), μ the dynamic viscosity, k the thermal conductivity, c_p the specific isobaric heat, R_0 the gas law constant, γ the coefficient of volumetric thermal expansion and ρ_0 the density at a reference temperature T_0. We assume no-slip conditions at all walls.

The boundary conditions for the temperature are as follows:

isothermal top and bottom wall:

$$T(r, \phi, 0) = T_{\mathrm{hot}}, \tag{5}$$

$$T(r, \phi, H) = T_{\mathrm{cold}}; \tag{6}$$

perfectly insulated lateral wall:

$$\partial T/\partial r\,|_{r=R} = 0. \tag{7}$$

Aspect ratio (height-to-diameter ratio), inclination angle α of the cylinder axis with the direction of the gravity field, Prandtl number and Rayleigh number can be optionally varied. The following scales for non-dimensionalization are used:

Rayleigh number:

$$\mathrm{Ra} = g\,\beta D^3(T_{\mathrm{hot}} - T_{\mathrm{cold}})/\nu\kappa.$$

Rayleigh number of pulse amplitude:

$$\mathrm{Ra}^* = g^*\,\beta D^3(T_{\mathrm{hot}} - T_{\mathrm{cold}})/\nu\kappa.$$

Prandtl number:

$$\mathrm{Pr} = \nu/\kappa.$$

Fourier number:

$$\mathrm{Fo} = t\kappa/D^2.$$

Fourier number of pulse duration:

$$\mathrm{Fo}^* = \hat{t}\kappa/D^2,$$

dimensionless velocity:

$$v^* = vD/\kappa,$$

dimensionless frequency:

$$f^* = fD^2/\kappa,$$

where D denotes the cylinder's diameter, t the time, $\hat{t}$ the pulse duration or period, β the compressibility, ν the kinematic viscosity and κ the thermal diffusivity.

2.2. Method of solution

Transient laminar natural convection inside a cylinder is studied by a three-dimensional calculation. The numerical code is based upon a finite-volume method with explicit time steps and a semi-iterative pressure and velocity correction [11]. The partial differential equations are discretized by using an equidistant mesh (Δr = constant, $\Delta\phi$ = constant, Δz = constant).

The algebraic finite-volume equations are formulated in dimensional variables (v_r, v_ϕ, v_z, p, T). Temperature and pressure are defined in the center of the finite volumes. The velocities are calculated for points that lie on the faces of the control volumes ("staggered grid").

Fig. 2 shows the grid arrangement and the locations of the velocity components in a radial and an axial cross-section. All properties except density, which is assumed to be temperature-dependent, are assumed to be time-independent and constant throughout the whole cylinder.

The whole flow field is calculated and then the maximum velocity at each time step is determined in order to describe the intensity of fluid motion. Even if location and direction of the maximum velocities vary, its magnitude is an upper limit for all velocities in the fluid. The general flow mode in a horizontal cylinder is one big roll with upstream at the hot and downstream at the cold wall. In the case of a cylinder with $H/D = 1$ the velocities adjacent to the hot and cold wall are of the same magnitude as the ones adjacent to the lateral wall.

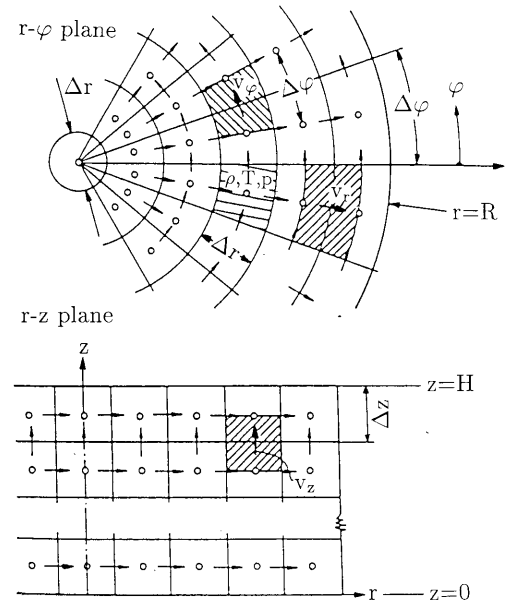

Fig. 2. Grid arrangement in the $r-\phi$ plane and $r-z$ plane.

So even if the maximum velocity is observed adjacent to the lateral wall it describes the velocities near to the hot and cold walls as well.

3. Calculation of g-jitter accelerations

3.1. Initial conditions

Because of the absence of gravity before application of the perturbation a fluid state of no motion ($v_r = v_\phi = v_z = 0$) and a constant pressure throughout the whole cylinder is assumed as an initial condition. A linear temperature gradient is applied from the bottom to the top ($\partial T/\partial z = (T_{cold} - T_{hot})/H$) due to heat conduction. In this study the aspect ratio of the cylinder is taken to be $H/D = 1$.

3.2. Single step pulses

A single gravity step of amplitude Ra* and duration Fo* is applied to the fluid. In a former study [10] we showed that in the case of an air-filled cylinder of aspect ratio $H/D = 1$ the ratio maximum velocity/Ra* is constant for a

fixed pulse duration Fo*. Furthermore the time constant of the decay of motion after fading of the gravity step is constant in the range of Rayleigh numbers investigated (Ra* = 200–5000). The decay constant is also independent of the pulse duration. Equivalent results are obtained for aspect ratios of 0.5, 2 and 5.

In this study we want to examine the influence of the Prandtl number. A horizontal cylinder ($\alpha = 90°$) filled with various fluids is exposed to gravity step pulses of amplitude Ra* = 5000 and infinite duration Fo*. The results are given in fig. 3, where the first dash-dotted line (1 dash + 1 dot) corresponds to liquid silicon (Pr = 0.023), the rigid one to air (Pr = 0.71), the dashed one to water (Pr = 7.0) and the second dash-dotted one (dash + 2 dots) to glycerin (Pr = 134.9). Fig. 3 also includes the case of single gravity pulses of finite durations Fo*, if only these parts of the graphs are considered that correspond to the specific pulse duration.

The glycerin flow reacts most to the gravity change. The overshoot is the largest in that case. But the development time of the steady state seems to be nearly the same as in the cases of air and water. Also the steady-state velocity is nearly constant for these three fluids. Only the flow in liquid silicon behaves quite different from that: There is no overshoot and the steady-state velocity reaches only 60% of the magnitude of the other fluids. Also the non-dimensional time (Fo) to reach the steady state is much larger.

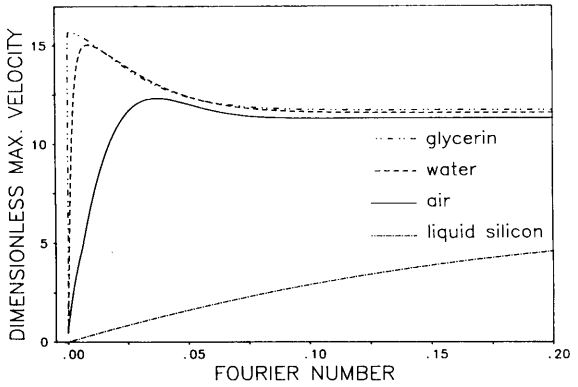

Fig. 3. Maximum velocity caused by a single gravity step of infinite duration (Ra* = 5000, $H/D = 1$, Fo* $\to \infty$).

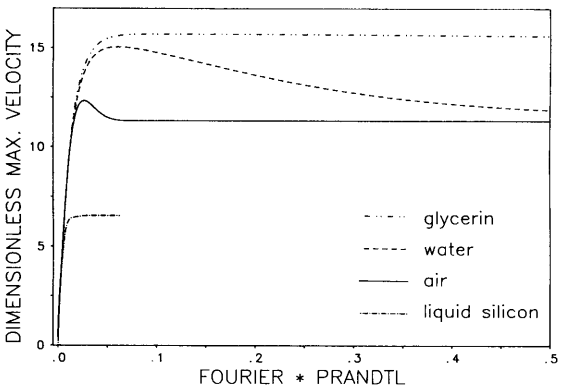

Fig. 4. Maximum velocity caused by a single gravity step of infinite duration (Ra* = 5000, $H/D = 1$, Fo* $\to \infty$).

In fig. 4 the horizontal axis is changed to Fo · Pr. This means a dimensionless time based upon the kinematic viscosity ν instead of the thermal diffusivity κ. By this the initial velocity increases are combined in one graph, but the maximum transient velocity is dependent on Pr.

Our results are summarized as follows:

- The transient maximum velocity depends initially only on Fo · Pr (see fig. 4). This means that the flow development is dominated by the viscosity of the fluid.
- For Pr ≥ 1 the time to reach the steady-state velocity is constant if it is expressed as a Fourier number (fig. 3). So the time to reach the steady-state velocity is depending on the thermal diffusivity.
- The velocity overshoots increase with increasing Pr (fig. 3) (and increasing Ra* (fig. 7)). For liquid silicon no overshoot is observed.
- The steady-state velocity is nearly independent of Pr for Pr ≥ 1. For the boundary conditions used here it is only a function of Ra*, for a given cylinder geometry. For Pr < 1 the steady-state velocity decreases with decreasing Pr.

3.3. Single sinusoidal pulse

Starting from a state of rest (see section 3.1) a sinusoidal gravity pulse of one period is applied to a fluid-filled horizontal cylinder ($g(t) = g^* \sin(\omega t)$, with $\omega = f/2\pi$). The gravity pulse is described by its amplitude Ra* and its period Fo*

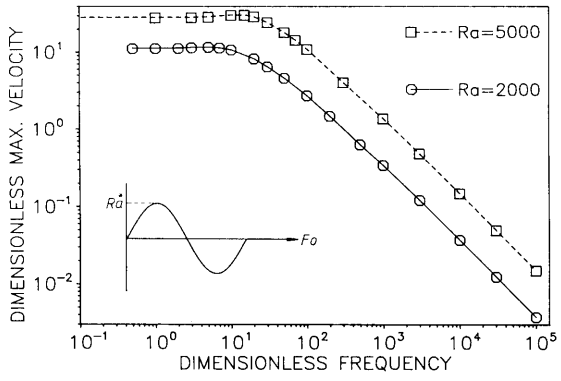

Fig. 5. Maximum velocity caused by single sinusoidal gravity pulses of various frequencies (Ra* = 5000 and 20000, H/D = 1, air, Pr = 0.71).

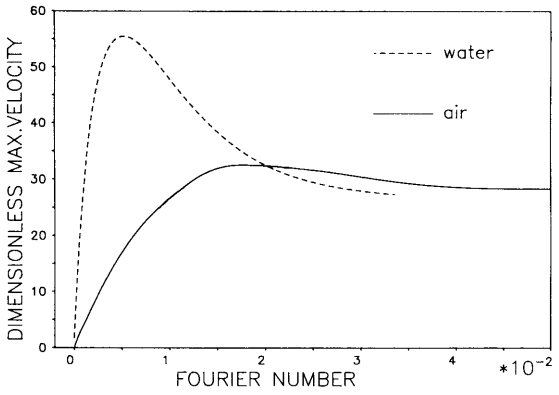

Fig. 7. Transient maximum velocity as response to a gravity step of infinite duration (Ra* = 20000, H/D = 1, air and water).

respectively the frequency f^* which is the reciprocal of Fo*.

Fig. 5 shows the dependence of the non-dimensional maximum velocity on the frequency for different Rayleigh numbers in the case of an air-filled cylinder (Pr = 0.71) and fig. 6 the same for a water-filled cylinder (Pr = 7.0). In both cases the maximum velocity is constant for small values of the frequency and decreases rapidly after a certain value of the frequency is exceeded. The rate of the decrease is independent of the Rayleigh number in the range investigated. The most striking difference between the two figures is the significant velocity maximum at frequencies just below the cut-off frequency in the case of water. This could be explained with the help of fig. 7 which shows

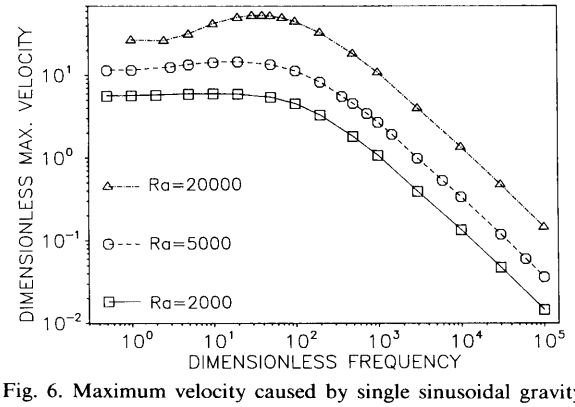

Fig. 6. Maximum velocity caused by single sinusoidal gravity pulses of various frequencies (Ra* = 2000, 5000 and 20000, H/D = 1, water, Pr = 7.0).

the fluid's reaction to a sudden change from zero-gravity to a constant gravity level of Ra* = 20000 (similar to section 3.2). While in air the transient velocity exceeds the steady-state value by about 14% the velocity in the water-filled cylinder overshoots by more than 100%. In the beginning the maximum velocity is observed near to the isothermal wall, then it appears in the vicinity of the lateral wall and moves towards the cylinder axis as the fluid motion develops (comparable to a developing boundary layer). In the steady state there is an S-shaped velocity profile in the midplane perpendicular to the cylinder axis ($z = H/2$).

When the sinusoidal excitation is considered to be composed of small amplitude steps, at low frequencies the velocity reaches the steady state after each step. At moderate frequencies the velocity might only reach a state near to the velocity maximum. At high frequencies the pulses succeed one another so quickly that the fluid cannot follow the excitation. Consequently, the overshoot could be interpreted as some kind of resonance behaviour between excitation and fluid motion.

Fig. 8 shows the fluid's reactions to sinusoidal pulses of Ra* = 5000 in the case of cylinders filled with liquid silicon (Pr = 0.023), air (Pr = 0.71) or water (Pr = 7.0).

It could be clearly seen that the rate of the velocity decrease with increasing frequency is independent of the kind of fluid respectively the Prandtl number. Also the magnitude of the veloci-

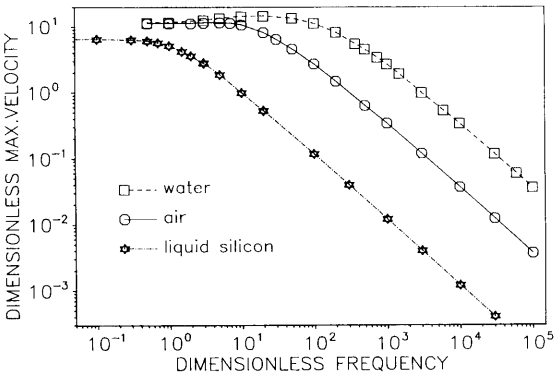

Fig. 8. Maximum velocity caused by single sinusoidal gravity pulses of various frequencies (Ra* = 5000, $H/D = 1$, liquid silicon, air, water).

ties at very low frequencies seems to be independent of the kind of fluid for $Pr \geq 1$. For liquid silicon these velocities are significantly smaller than for air or water. This agrees with the results in section 3.2. The value of the cut-off frequency is linearly dependent on Pr as it is shown in fig. 9. Here the frequency is divided by Pr and this leads to one graph for all the fluids investigated. Only in the frequency range below the cut-off frequency does the magnitude of the overshoot depend on Pr ($Pr \geq 1$) or in the case of $Pr < 1$ the velocities vary with Pr. As Kirchartz et al. [7] have calculated, the amplitude of the overshoot for the case of a rectangular cavity increases with increasing Pr while the rate of the overshoot's increase decreases with increasing Pr. With increasing Ra* the magnitude of the overshoot increases and also the frequency of its occurrence slightly increases.

3.4. Series of step pulses of alternating direction

A horizontal cylinder is subjected to an infinite series of step pulses of alternating direction as sketched in fig. 10. When the velocities have reached the steady-state of oscillation the maximum velocity is recorded. The graphs of fig. 10 show these velocities caused by gravity steps of amplitude Ra* = 5000 in cylinders filled with air, water or glycerin. The frequency is defined the same way as in the case of the sinusoidal pulses: 1 period consists of a positive and negative step.

For low frequencies after each change in gravity the steady state is reached. For such frequencies the velocities observed are approximately the same as for a single step (see section 3.2). For higher frequencies the velocities at the steady state of oscillation are up to 50% less than in the case of the single step pulse of equivalent pulse duration as the "initial condition" after each step is a flow of opposite direction than the one excited by the new gravity direction. So the time for developing the new flow is reduced by the initial damping of the old flow. The cut-off frequencies of the various fluids are approximately the same as the ones mentioned in the latter sections. (They are slightly higher than in the case of a single pulse.)

If the frequency is divided by Pr, the parts of the graphs of fig. 10 that describe the velocities at

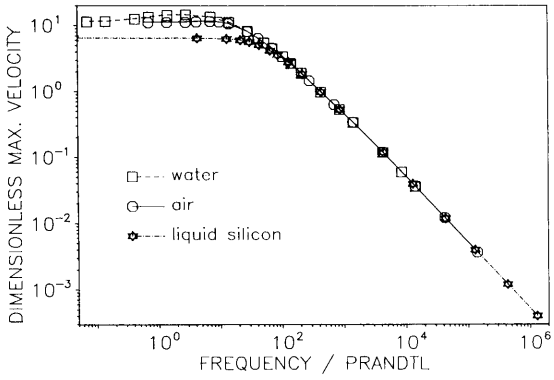

Fig. 9. Maximum velocity caused by single sinusoidal gravity pulses versus frequency/Pr (Ra* = 5000, $H/D = 1$, liquid silicon, air, water).

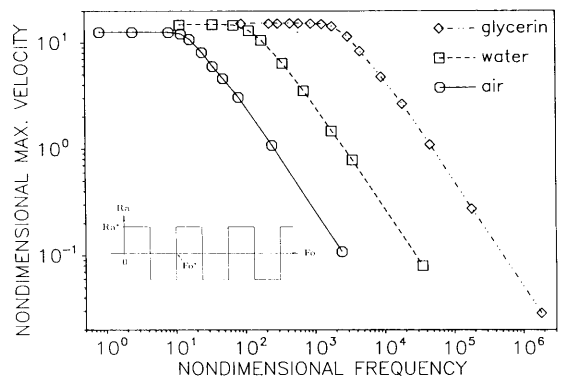

Fig. 10. Steady-state of oscillation maximum velocity caused by gravity steps of alternating direction (Ra* = 5000, $H/D = 1$, air, water, glycerin).

higher frequencies can be summarized in one graph in the same way as in fig. 9. At small frequencies there are differences between the velocities of the various fluids due to the different sensitivities to gravity pulses as mentioned in section 3.2 (fig. 3).

3.5. Gravity vector rotating in the r-z-plane

This interference means a continuous change of the inclination angle α (see fig. 1). The cylinder is supposed to be fixed with respect to the spacecraft. Only the gravity vector is rotating, there are no centrifugal forces acting on the cylinder and the fluid. The flow inside the cylinder changes its direction twice every period. Fig. 11 shows the dependence of the maximum velocity in the steady state of oscillation on the frequency for an air-filled cylinder at Ra* = 2000 and 5000 and for a water-filled cylinder at Ra* = 5000. The general behaviour is the same as in the cases described yet. At low frequencies the fluid can follow the gravity vector so that the steady state is nearly reached at every inclination angle. At high frequencies the fluid motion cannot follow the gravity vector. At the cut-off frequency, however, the overshoots are much smaller than in the case of the sinusoidal pulse. For water the velocity overshoots by about 10%. In the case of air the overshoot is very small (2%) at Ra* = 5000 and in the case of Ra* = 2000 no overshoot is observed. (This small overshoot could also be caused by the discretization as the place where the maximum velocity is observed

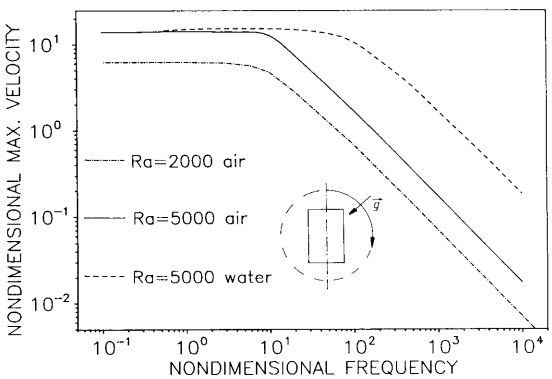

Fig. 11. Steady-state of oscillation maximum velocity caused by a gravity vector rotating in the $r-z$ plane (Ra* = 2000, air, Ra* = 5000, air and water, $H/D = 1$).

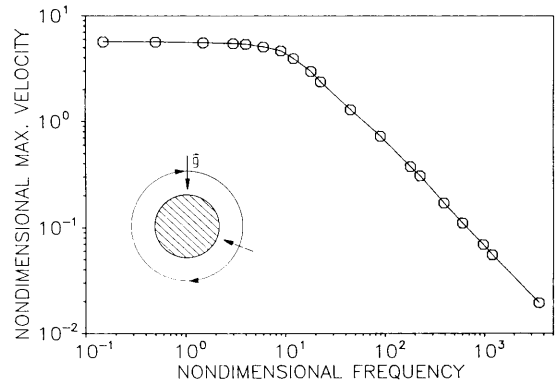

Fig. 12. Steady-state of oscillation maximum velocity caused by a gravity vector rotating in the r–ϕ plane (Ra* = 2000, $H/D = 1$, air).

moves during flow development.) Again the rate of the velocity decrease for increasing frequencies above the cut-off frequency is independent of Ra* and Pr. And the cut-off frequency of water is about ten times the one of air at the same Ra*.

3.6. Gravity vector rotating in the r-ϕ-plane

A horizontal air-filled cylinder is subjected to a gravity vector rotating in the $r-\phi$ plane. That means the gravity vector is always perpendicular to the cylinder axis and is rotating around it. The cylinder itself does not rotate. So there are no rotations applied to the fluid by the walls.

The general shape of the graph (fig. 12) seems to be the same as the last one (fig. 11) even if the kind of excitation is very different. Here the flow is forced to rotate perpendicular to the main flow direction that is parallel to the lateral wall. There is no gravity force acting in or against the main flow direction. The cut-off frequency is found with a value of $f^* \approx 10$. No resonance frequency is found.

4. Conclusion

By using a numerical code the laminar three-dimensional buoyancy-driven flow in a differentially heated cylinder is studied. Various kinds of g-jitter perturbations causing this convection are investi-

gated. In terms of the Fourier number (a dimensionless time) a fluid is more sensitive to a gravity pulse for high Prandtl numbers. Also, for the higher Pr and Ra* (Rayleigh number of pulse amplitude) there is more tendency for the transient velocity to overshoot the steady-state velocity. The latter is nearly constant for fluids with $Pr \geq 1$, but decreases with decreasing Pr when $Pr < 1$.

In general, high-frequency *g*-jitter perturbations can be ignored when they occur together with low-frequency perturbations. The influence of *g*-jitter is difficult to estimate in general. But especially in the case of quite large dimensions of a cavity, *g*-jitter perturbations should be taken into account as Ra* increases with the third power of the diameter. With the given sensitivity criterion, i.e. velocities should be kept to a minimum, it appears that the cylinder should be positioned in such a direction that the largest transient *g*-jitter perturbations act parallel to the cylinder axis and so in the direction of the temperature gradient. The fluid flow is much more insensitive to gravity pulses in this case (see section 1). An isolation from the transient pulses might be also considered.

In this study we wanted to show the influence of some parameters that describe thermal convection caused by *g*-jitter perturbations. Our mathematical model could be extended to several other effects dependent on the requirements of specific applications. For instance, it is possible to take into account effects like concentration distributions and diffusion, different boundary conditions (e.g. surface-tension-driven convection on free surfaces) or geometries and many effects related to the solid–liquid interface and solidification.

References

[1] J.W. Elder, J. Fluid Mech. 35 (1969) 417.
[2] T.D. Foster, J. Fluid Mech. 37 (1969) 81.
[3] P.M. Gresho and R.L. Sani, J. Fluid Mech. 40 (1970) 783.
[4] R. Monti, D. Langbein and J.J. Favier, in: Fluid Sciences and Materials Sciences in Space, Ed.. H.U. Walter (Springer, Berlin, 1987).
[5] P.R. Griffin and S. Motakef, Analysis of the Fluid Dynamics and Heat Transfer During Micro-Gravity Bridgman–Stockbarger Growth of Semiconductors in Steady Periodic Gravitational Fields (ASME Technical Paper 87-WA/HT-1, New York, 1987).
[6] K.R. Kirchartz, in: Spacelab-Nutzungen, Statusseminar 1982 des Bundesministerium für Forschung und Technologie (1982) pp. 43–59.
[7] K.R. Kirchartz, H. Oertel, Jr. and J. Zierep, in: Convective Transport and Instability Phenomena, Eds. J. Zierep and H. Oertel, Jr. (Braun, Karlsruhe, 1982) pp. 101–122.
[8] K. Kueblbeck, G.P. Merker and J. Straub, Intern. J. Heat Mass Transfer 23 (1980) 203.
[9] A. Heiss, Numerische und experimentelle Untersuchungen der laminaren und turbulenten Konvektion in einem geschlossenen Behälter, PhD Thesis, Technische Universität München (1987)
[10] St. Schneider, T. Heiss and J. Straub, in: Proc. Intern. Symp. on Thermal Problems in Space-Based Systems, ASME HTD, Vol. 83, Eds. F. Dobran and M. Imber (ASME, New York, 1987) pp. 77–83.
[11] S.V. Patankar, Numerical Heat Transfer and Fluid Flow (McGraw-Hill, New York, 1980).